4

Anisotropic superhydrophobicity and unidirectional droplet rolling

In the previous chapter, we explored isotropic wettability of abaxial Indian jujube leaf surfaces, where droplets exhibited uniform wetting behaviour. In this chapter, we focus on anisotropic wettability of natural leaf surface, which has gained interest for its potential in unidirectional droplet control. To investigate this, the surface of the natural sword lily (Gladiolus hortulanus) leaf and bio-mimicked polystyrene (PS) construct were closely examined, with particular attention to microstructures and roll-off conditions. Additionally, a relevant theoretical framework is highlighted.

4.1 Introduction

The wetting state of a solid surface is typically evaluated by measuring the static contact angle (CA) of a liquid droplet (e.g., water) placed on it, where the droplet forms a uniform CA along the three-phase contact line (TCL), indicating isotropic or symmetric wetting. When a droplet is deposited on a surface with heterogeneous physical or chemical textures, the contact line becomes non-uniform. This leads to asymmetric wettability, known as anisotropic wetting (see Appendix I, (Fig. A.1(b))). Such behavior is often observed on striated patterned solid surfaces featuring both hydrophilic and hydrophobic responses [178, 179]. In nature, many plants and insects have textured surfaces that are capable to show anisotropic wetting, such as rice leaves, butterfly wings, and water strider legs [28, 180]. The surface of a rice leaf exhibits a three-level hierarchical structure (macro, micro, and nano) and displays anisotropic wetting behaviour [181]. When a droplet rolls on a slanted rice leaf, it follows a specific directional path. As discussed in the previous chapter, isotropic surfaces like those of lotus [10], taro [82], and silver ragwort [88] leaves cause droplets to shed randomly on slanted surfaces. In contrast, anisotropic

wetting enables droplets to move along a guided track [182]. These features enable water droplets to readily roll-off the surface unidirectionally, an effect recognized as anisotropic droplet rolling, or dewetting [183]. Inspired from such features, numerous researchers have undertaken steps to replicate three -level surfaces while focussing anisotropic wetting characteristics coupled with self-cleaning attributes. A vast amount of efforts was put into engineering artificial surfaces that could mimic these single and multiscale hierarchical structures substantially [17, 91, 184–188]. This endeavour has been pursued through various fabrication techniques, including laser patterning [187, 189, 190], electrospinning [191], photolithography [90], mechanical surface wrinkling [185, 192] etc. These techniques enable the creation of surfaces with tailored anisotropic wetting properties, often designed to achieve static wetting anisotropy, or to induce controlled droplet motion.

Researchers have developed specialized surfaces featuring hierarchical structures inspired by superhydrophobic rice leaves [17, 90, 181]. The biomimetic surface inspired from rice leaf was also discussed with controllable droplet sliding angle for structures with different periodicity [181]. Moreover, the rice leaf inspired mimicked wavy surface was created by using a layer-by-layer deposition technique with surface wrinkling of different surface roughness [17]. Over the years, researchers have consistently strived to replicate natural surfaces with reasonable success, but due to the intricate structures present at the micro-nano scale, achieving flawless imitation remains an ongoing endeavour. The findings of anisotropic wetting in rice leaves and butterfly wings have inspired attempts to bio-mimic and replicate artificial surface designs with much needed anisotropic wettability [17, 181, 193].

In this chapter, we studied the anisotropic superhydrophobic wettability aspect of the adaxial leaf surfaces of sword lily (*Gladiolus hortulanus*) being characterized by dynamic WCA and roll off angle measurements in parallel and perpendicular directions to the leaf-midrib. The three-level structure with micro-nano hierarchical makeups has also been replicated as part of bio-mimicking process using low molecular weight polyvinyl alcohol (PVA) and polystyrene (PS) as negative, and positive replica; respectively. The natural sword lily leaf surface and bio-mimicked PS constructs were examined with care, emphasizing microstructure and roll off conditions. In addition, a theoretical treatment is also considered and highlighted.

4.2 Experimental procedure

4.2.1 Sample collection and preparation

The sample collection, preparation, and precautions are similar to those discussed in the section (3.3.1). The fresh natural sword lily leaf samples were collected locally

from one of the nearby village nurseries. The samples were placed in the glass petri dish carefully in ambient environment and subjected to air blow to remove away common particulate contaminants like mist, dust, pollen etc. The size (length × width) of the leaf under study was ∼50 × 2 cm^2, and for characterization of wettability features, at least three specimens were chosen. They were gently cut into ∼20 × 10 mm^2 pieces as per need and then, affixed on the microscope glass slide with the help of a double-sided adhesive tape.

4.2.2 Surface morphology and biomimicking through soft lithography

The surface morphologies of the natural adaxial sword-lily leaves and artificially made (bio-mimicked) leaf replicas were captured using a field emission scanning electron microscope (*JEOL®, FE-SEM, JSM 6390LV*) at varied magnifications. For FE-SEM imaging characterization, the samples were segmented into smaller sizes of ∼5 × 5 mm^2, and then several nanometers of platinum were sputtered onto them to prevent the charging effect, making the surface evenly conducting. The abaxial and adaxial surface textures were compared for similarity using a microspectrophotometer (*RIMS®-RT-VIS/NIR-BX43*). Surface roughness was also characterized using a surface profilometer (*Taylor Hobson, Ametek Technologies®*), for which the samples were segmented into smaller sizes of ∼10 × 15 mm^2 and fixed onto microscope glass slides with double-sided tape. Data acquisition was performed by scanning over the specimen along both the parallel and perpendicular directions of interest. Lastly, the surface profilometer used a stylus probe with a diameter of ∼5.94 μm and an overall sampling length of ∼7.98 mm.

In soft lithography, a negative replica is created by moulding a water-soluble polymer (PVA) or epoxy [26, 194]. Subsequently, a positive replica is formed by pouring polystyrene (PS) or an elastomer like PDMS into the template. A stepwise description for creating a biomimicked superhydrophobic surface texture of the sword lily leaf under study is illustrated in Fig. 4.1. The primary concern was to optimize the mimicking steps in order to accurately replicate the leaf surface. The bio-mimicking process was conducted in two main steps, as shown in Fig. 4.1. In step 1, the sword lily leaf surface was used as a template to create a PVA negative replica. For this, the adaxial sword lily leaf template was fixed to the bottom of an open, wide glass container such that the surface to be mimicked was in an upright position. The ∼10 wt.% polyvinyl alcohol (PVA, Mw ∼125,000, CDH®) solution with DI water was poured slowly onto the fresh leaf template in an ambient environment. The PVA solution filled the micro-nano voids of the leaf texture. After mild drying, the glass container was kept in a glass vacuum desiccator (pressure ∼600 mm Hg,

24 h) to remove the undesired air trapped at the PVA-leaf interface. Once the bubbles were eliminated, the glass container with the PVA film was dried at room temperature for nearly 48 hours. After the complete evaporation of water, the PVA layer was peeled off the lily leaf template, resulting in a bio-mimicked PVA negative replica. In step 2, this PVA negative replica served as a new template and was then treated with a ~10 wt.% polystyrene (PS, Mw ~280,000, Sigma-Aldrich®) solution in chloroform (Mw ~119.38, Sigma-Aldrich®) solvent. The PS-deposited template was kept in a vacuum desiccator for ~24 h. After allowing it to dry for the whole day at a temperature of ~45°C, the PS layer was gently peeled off the PVA base using small forceps or tweezers. Consequently, the PS positive replica is produced as a bio-mimicked PS construct version of the natural sword lily leaf surface.

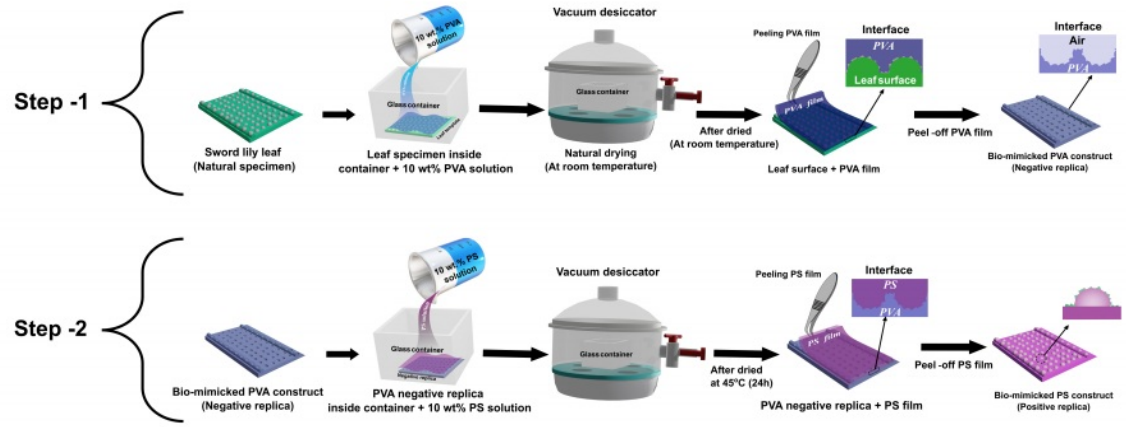

Figure 4.1: The scheme illustrates the series of steps (1 and 2) for biomimicking process of natural lily leaf surface. In step -1, adaxial sword lily leaf surface serves as a template to develop PVA negative replica. In step -2, the bio-mimicked PVA negative replica as a template to develop PS positive replica as a bio-mimicked PS construct.

4.2.3 Anisotropic wettability measurements

The WCA measurements were carried out with different droplet volumes (~4-10 μL) by employing the popular sessile drop method on an advanced Contact Angle Meter setup (*Kyowa Interface Science®, Japan*) as discussed in section (3.3.2). Moreover, for static and dynamic WCA characterization of striated natural sword-lily leaf and positive (PS) surface in orthogonal (parallel (striated) and perpendicular) directions, only the substrate base was rotated in the horizontal (x-y) plane as needed, without disturbing the light source and camera setup, as can be found in Fig. 4.2(a). The static WCAs in both directions ($\theta_{\parallel}$ and $\theta_{\perp}$) were measured by rotating the template (leaf)-supported stage in the horizontal plane, as shown in Fig. 4.2(b). The dynamic WCAs were measured by rotating the light-camera-substrate stage as per need. The specimen stage was tilted vertically up to a tilting angle, $\alpha \sim 90°$ (Fig. 4.2(a)).

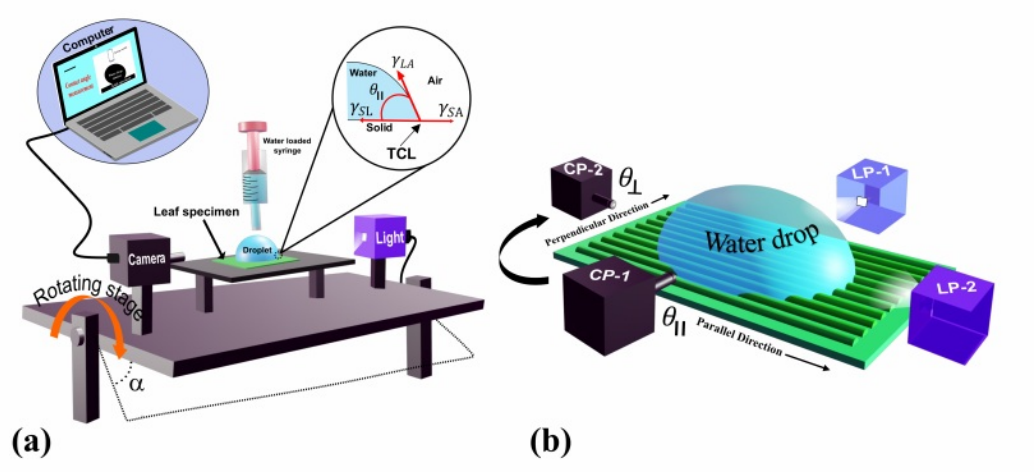

Figure 4.2: (a) Schematic of static and dynamic WCAs measurement setup for measuring anisotropic wettability on textured surface. The rotating stage offers tilting angle of specimen from α ~0°-90° (not to scale with the experimental specimen). (b) Schematic illustration of WCA along parallel and perpendicular directions upon placing the water droplet on the striated surface. The curved black arrow represents the rotation of specimen in the horizontal plane with different positions of camera (CP1 and CP2) and light source (LP1 and LP2) which help measure WCAs along parallel and perpendicular directions.

All the WCA measurements and surface profiling were performed in ambient environment, at a temperature of 300 K.

4.3 Morphology of sword lily leaf surface and biomimicking

4.3.1 Natural sword-lily leaf surface

Different parts of the sword lily leaf surface, on both the sides of adaxial (upper) and abaxial (lower) parts, to a great extent, exhibit alike features as regards surface morphology and wettability due to isobilateral (equi-facial) effect [195]. A close digital photograph of natural sword-lily plant can be found in Figs. 4.3(a) and 4.3(b). The small black and red arrows indicate the respective abaxial and adaxial sides of the leaf surfaces, whereas optical micrographs of both sides are shown in Figs. 4.3(c) and 4.3(d). Indicated by a yellow arrow the leaf exhibits symmetry along the midrib, while the inset depicts the dewetting feature of the leaf surface (Fig. 4.3(a)). A selected area of the adaxial surface is specified by a yellow rectangle labelled "1", the magnified version of which is shown in Fig. 4.3(b). The region of the leaf surface chosen for further characterization is indicated by a cyan rectangle marked "2" in Fig. 4.3(b), and the FE-SEM image of this region being shown in Fig. 4.4. It is important to note that micro-striations can vary both in size and separation, which refers to changes in the height of the striations and the distance between successive parallel

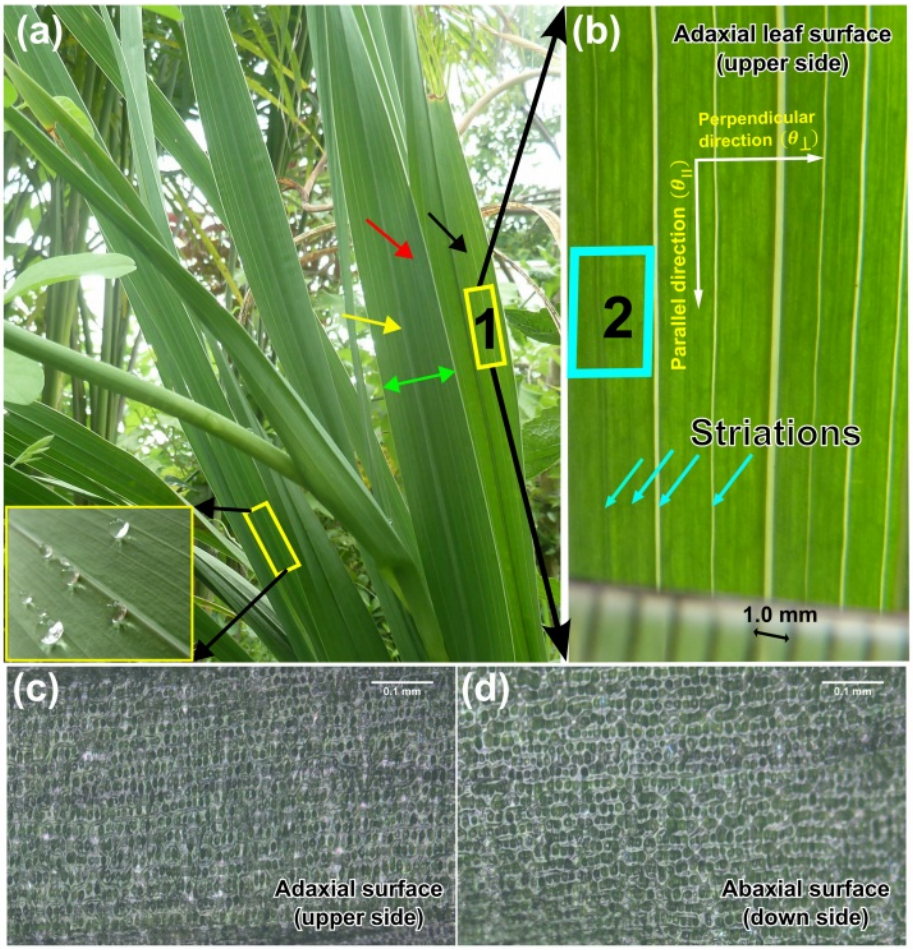

Figure 4.3: (a) The photographic image of sword lily plant. The magnified top view of leaf surface holding water droplets is shown as inset. The small black, red, yellow, and green arrows indicate the adaxial side, abaxial side, midrib, and width of the leaf surfaces; respectively. (b) The magnified digital image of the adaxial sword lily leaf surface. (c) and (d) are the optical microscopic image of adaxial (upper) and abaxial (down) side of sword lily leaf surface.

striations. Much like in certain plants and insects [28, 181, 196], the surface of the sword-lily leaf was believed to be composed of three-levels of structures: micro-scale striation, micro-protrusions (micro-papillae) and nano-scale waxy flakes (Figs. 4.4(a-c)). It is interesting to note that the micron-scale striations and the spaces between them are covered with organized micron-scale protrusions (Figs. 4.4(a) and 4.4(b)) and these micro-protrusions are covered with nano-scale waxy flakes over the leaf surface (Fig. 4.4(c)). Also, the striations and the area between them are covered with nano-sized waxy structures. However, these micro protrusions are quite well ordered with arrays several micrometres apart in parallel and perpendicular directions, respectively (indicated by the respective symbols $\parallel$ and $\perp$, Fig. 4.4(a)). The arrays of strips can be seen with typical spacing approximately, $\sim$500-700 μm as depicted in FE-SEM image (Fig. 4.4(a)). Apparently, the three-levels of surface texture with unique striated structures and specific arrangements of micro protrusions (papillae) covered with waxy flakes are believed to be responsible for the observed

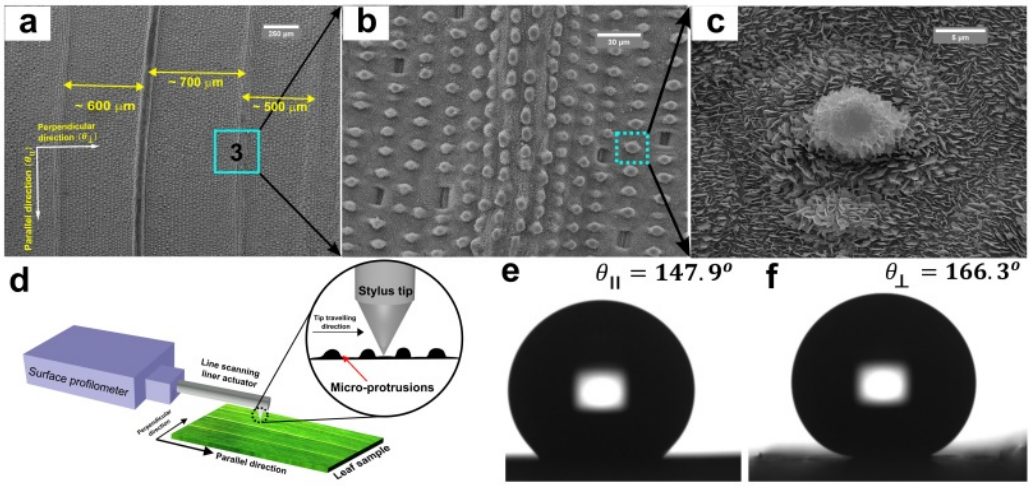

Figure 4.4: (a, b) High resolution FE-SEM image captured at specific region of the lily leaf surface (see 4.2(b)). (c) Magnified FE-SEM image of micro protrusions covered with nano waxy flakes. (d) Schematic of surface roughness measurement of leaf surface. (e, f) Optical image of the wetting state of the water droplet on lily leaf surface along parallel ($\parallel$), and perpendicular ($\perp$) directions; respectively.

anisotropic superhydrophobicity phenomenon. The micro-papillae appear with an elliptical shape (top view), with a typical major axis of ∼5 μm and a minor axis of ∼3.5 μm, as predicted from the FE-SEM imaging and analysed through *ImageJ* software. The arrangement of papillae gives a minor axis along parallel (striation) direction and a major axis along perpendicular direction, with respective separations ∼3-15 μm and ∼10-17 μm (Fig. 4.4(b)). The micro-protrusions as well as vacant surfaces between protrusions are largely covered with waxy nano flakes with average heights ∼270-750 nm and thicknesses ∼40-76 nm.

The micro-texture parameters were analysed using a surface profilometer, depicted in schematic Fig. 4.4(d). The measurements were carried out along parallel and perpendicular directions of the leaf surface. Based on standard deviation from height distribution calculations, the root-mean-square (rms) roughness, R_q profiling was found in the range ∼1.5-2.0 μm and ∼15.1-16.6 μm along parallel and perpendicular directions; respectively (see Appendix II, Figs. (A.7) and (A.8), (table (T.2) and (T.3)). With a sampling length of ∼7.98 mm, when the stylus tip was allowed to scan over the parallel direction, only micro-protrusions contribute largely to the roughness since the waxy flakes are of nano-scale dimensions. The rms roughness in the perpendicular direction is influenced by the micron-scale striations and along with adequate protrusions. There is a noticeable difference in the roughness of the leaf surface when measured in different directions namely, perpendicular and parallel directions, respectively. Specifically, the R_q value is much higher by about ∼13.5 μm along perpendicular to the leaf's striation as compared to its value along parallel direction. This increased roughness is chiefly due to the micron-scale striations on the leaf surface. In other words, the heights of the striated bulging structure largely

contribute to the augmented rms roughness and consequently, would create an impregnable barrier to the droplet motion along the perpendicular direction. The state of water droplet, with a volume of $\sim$6 μL, on the sword lily striated leaf surface is depicted in Figs. 4.4(e) and 4.4(f), corresponding to the parallel ($\theta_{\parallel}$) and perpendicular ($\theta_{\perp}$) directions, respectively.

4.3.2 Biomimicking of sword-lily leaf surface

The natural leaf with micro and nano sub-surface textures serves as an ideal testbed for developing bioinspired construct through artificial means. Here, the sword lily leaf surface with distinct surface morphologies is our relevant template for anisotropic superhydrophobicity and roll-off characteristics. As an alternative to photolithography, this is achieved via a soft lithography technique that relies on self-assembly and appropriate moulding to develop micro- and nano-texturing in the replication process. This technique offers a convenient and efficient approach for creating rough and textured surfaces close to original system. Here, the sword-lily leaf top surface (adaxial side) is the main template, with a hydrophilic polymer (PVA) as negative replica stamp, and a hydrophobic polymer (PS) to offer as positive replica eventually. A stepwise description for creating optimized biomimicked superhydrophobic surface texture of the sword lily leaf has been discussed in section 4.2.2 (see Appendix II).

Exhibiting three levels of micro and nano texture, the FE-SEM images of sword-lily leaf surfaces at different magnifications can be found in Figs. 4.5(a-d). The negative replica of natural sword lily leaf surface texture imprinted on PVA surface is shown in Figs. 4.5(e-h). The magnified negative replica of micro protrusion (dotted green circle) on PVA film is shown in Fig. 4.5(f), whereas, the waxy texture of nano flakes of the leaf surface is invariably engraved on the PVA film as can be found in Figs. 4.5(c, g). It can be noticed that, the bio-mimicked PS surface construct offers reasonable exactness resembling natural leaf surface texture (Figs. 4.5(i-l)). Apparently, the micro-level mimicking is well-executed, but there is a shortfall in nano-texture replication (Figs. 4.5(b) and 4.5(j)). To be mentioned, the natural sword lily leaf surface micro protrusion is entirely covered with waxy nano-flake layer whereas the PS surface protuberance is covered with a sparse and scattered nano flakes. Also, as can be seen from Figs. 4.5(c) and 4.5(k), the non-protrusion area marked with dotted yellow rectangular unit in natural leaf specimen is covered with waxy nano flakes. Although the bio-mimicked PS construct provides a considerable degree of microstructural replication, but the nanostructures could not be replicated precisely as those on the natural leaf template. Consequently, the developed PS surface texture would exhibit competitive droplet rolling depending on the size of the droplet, and not as effective as natural leaf specimen. Nevertheless, the bio-mimicked

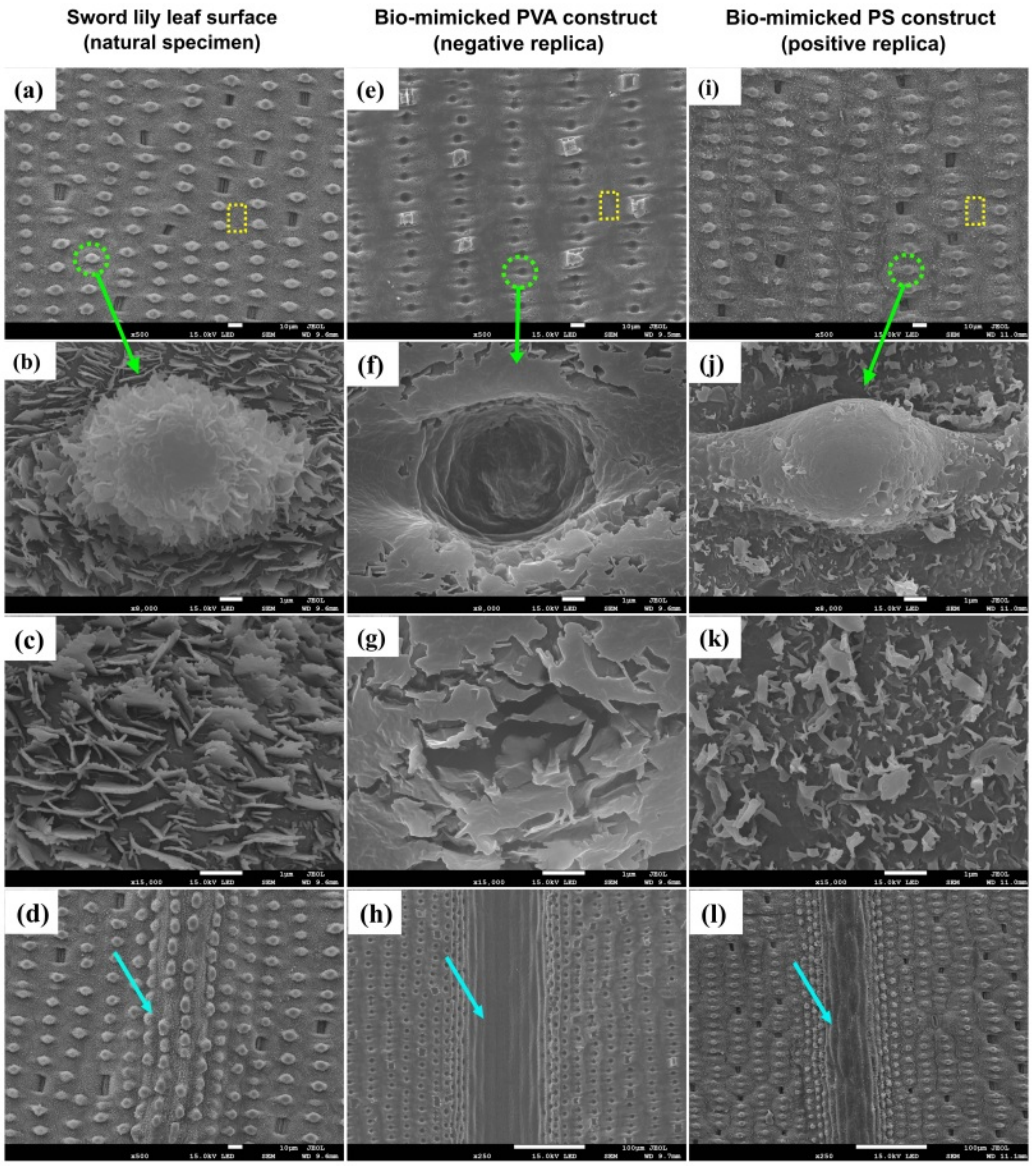

Figure 4.5: (a-d) High resolution FESEM images of natural adaxial lily leaf surfaces with different magnifications. The dotted circle (green) and rectangular (yellow) regions show micro-protrusions and flat-surface region between protrusions, respectively. The arrows (light blue) indicated the micro-scale striation. (e-h) Bio-mimicked PVA construct negative replica of leaf surface structure. (i-l) Bio-mimicked PS surface construct (PS positive replica).

final replica would emerge with three levels of surface texture as they exist in natural leaf surface.

The distinct micron-scale striation is indicated in Fig. 4.5(d). The negative and positive replica constructs being shown in Figs. 4.5(h) and 4.5(l), respectively. The PVA and PS film thicknesses, the depth of the striations engraved on the PVA, and the height of the striations on the bio-mimicked PS construct were estimated through the cross-sectional image analysis using *ImageJ* software. The measured thickness is likely to vary with each attempt on mimicking, depending on the amount of PVA (or, PS) solution poured over the templates. The thickness of the mimicked PVA and PS

films ranged from ∼80 μm to ∼350 μm on different attempts. The engraved depth on the PVA and the heights on the PS replica of the striations ranged from ∼60μm to ∼80 μm.

4.4 Static and dynamic WCA characterization of natural and bio-mimicked sword lily leaf surfaces

4.4.1 Anisotropic superhydrophobicity

The static average WCAs were measured in different regions of the specimen surfaces along parallel and perpendicular directions using contact angle meter as discussed in section 4.2.3. The WCA features were thoroughly examined for natural sword-lily leaf surface, along with bio-mimicked PS surface construct with lotus (*Nelumbo nucifera*) leaf surface as reference for isotropic superhydrophobicity. We have chosen lotus leaf as a reference surface due to its well documented isotropic superhydrophobicity with self-cleaning property [10] (surface morphology can found in Appendix II, Fig. (A.9)).

For a given water droplet volume ($\sim 6\,\mu L$), the WCA along the parallel ($\theta_{\parallel}$) and perpendicular ($\theta_{\perp}$) directions of sword-lily leaf can be found as $\sim$ 147.9° and ∼166.3°, respectively (Figs. 4.4(e) and 4.4(f)). To be mentioned, the WCA along the perpendicular direction is seemingly more superhydrophobic compared to the parallel direction, yet self-cleaning action becomes apparent in the latter case because of the existence of parallel striation with micro-protrusions and nanoscale surface geometry. While pinning action does not allow self-cleaning to occur along the perpendicular direction, the roll-off angle was seen to vary with droplet volume (size) along the parallel direction [17]. This discrepancy, seen as special characteristics, has conventionally been attributed to the parallel striation with the alignment of micro-papillae along the striation direction, and can be observed from the FE-SEM images (Figs. 4.4(a-c)). The measured WCAs show distinct values, indicating anisotropic superhydrophobicity attributed to a multi-scale surface texture. Micron-scale parallel striations create height barriers in the perpendicular direction, which enhances wetting anisotropy. Meanwhile, micro-protrusions and nano waxy flakes profoundly contribute to superhydrophobicity in both directions by entrapping air beneath the droplets within the texture. Consequently, the sword lily leaf surface displays a three-tiered structure that leads to a Cassie's suspended wetting state.

The response of WCAs with increasing droplet size ($\sim 4-10\,\mu L$) for parallel ($\theta_{\parallel}$) and perpendicular ($\theta_{\perp}$) directions for natural lily-leaf and bio-mimicked PS surface construct can be found in Fig. 4.6(a). As can be observed, for a droplet volume

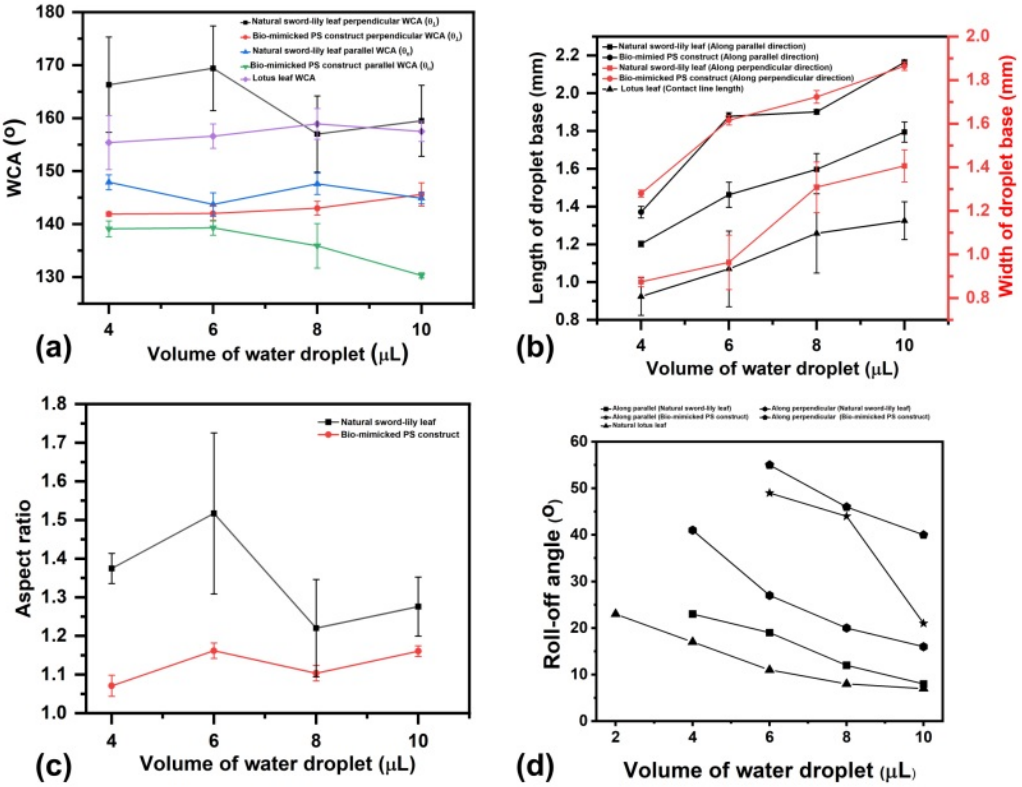

Figure 4.6: (a) WCA vs. droplet size plots for natural adaxial sword-lily leaf and bio-mimicked PS construct along parallel and perpendicular directions, respectively. The WCA response of natural lotus leaf is also shown as reference. (b) The plot of droplet volume dependent contact line (length and width) along parallel and perpendicular directions, respectively. Also, contact length of natural lotus leaf is shown as reference. (c) Droplet volume dependent aspect ratio plots for natural adaxial lily leaf and bio-mimicked PS construct surfaces, respectively. (d) Volume dependent droplet roll-off angle for the specimens under study with lotus leaf as reference.

change in the range $\sim 4-10\,\mu$L, the respective WCAs of sword lily surface tend to vary in the range, $\theta_{\parallel} \sim 143^{\circ}-147^{\circ}$, $\theta_{\perp} \sim 156^{\circ}-169^{\circ}$. In contrast, the PS replica offers WCAs viz. $\theta_{\parallel} \sim 130^{\circ}-139^{\circ}$ and $\theta_{\perp} \sim 142^{\circ}-145^{\circ}$. Noticeably, the bio-mimicked PS surface seems to exist in the borderline of hydrophobic and superhydrophobic region and with lower WCA than its natural lily leaf counterpart. Moreover, the WCA along the perpendicular direction experiences relatively higher values than along the parallel direction, thereby offering adequate anisotropic hydrophobicity. Even then, the dewetting-led droplet rolling action along the striated direction, i.e., along the parallel direction, is more favourable than the perpendicular direction on the leaf surface. Usually, superhydrophobicity is discussed in relation to self-cleaning features, and a higher WCA would characterize stronger self-cleaning activity. Whereas the lotus leaf exhibits isotropic superhydrophobicity, our sword-lily leaf specimen, even though the WCA is good enough in the perpendicular direction, it is less likely to roll off easily due to the pinning effect. One can also notice the effect for the droplets with larger volumes and that the WCA along the perpendicular direction of the leaf surface is quite comparable with the isotropic WCA of the lotus leaf texture. Moreover,

the bio-mimicked PS construct surface exhibits significant anisotropic hydrophobicity for given droplet volumes, though the sword lily leaf surface demonstrates even better anisotropy with superhydrophobicity. We invoke anisotropic wettability based on two characteristic parameters: first, the difference in WCA ($\Delta\theta$) along two mutually perpendicular directions and second, the ratio of their contact lines (aspect ratio, ζ) along parallel and perpendicular directions. The anisotropy, measured as a consequence of the difference in WCA ($\Delta\theta = \theta_{\perp} - \theta_{\parallel}$), is of course dependent on the size of the droplet ($\sim 4 - 10\,\mu$L): the range being $\Delta\theta \sim 9^{\circ} - 25^{\circ}$ and $\Delta\theta \sim 2^{\circ} - 15^{\circ}$ in the case of the natural leaf surface and bio-mimicked PS construct, respectively. The variation in length, l, and width, w, of the droplet cap in contact with the base on the surfaces of interest for different droplet sizes is shown in Fig. 4.6(b). We assume the length to be measured exactly along the parallel striation direction and the width along the perpendicular direction. The plot of aspect ratio ($\zeta = l/w$) vs. water droplet size is depicted for natural lily leaf and bio-mimicked PS construct surfaces in Fig. 4.6(c). This measurement quantifies the extent of anisotropic wetting behaviour exhibited by the droplet on the microtextured surfaces under study. From Figs. 4.6(a) and 4.6(c), it can also be realized that the natural lily leaf surface would favour low wetting area with high anisotropic dewetting feature compared to the bio-mimicked PS surface construct.

4.4.2 Droplet roll-off and contact angle hysterisis

To explore the dynamics of water droplets, the roll-off measurement with different droplet sizes were conducted for the lotus leaf, sword lily leaf, and bio-mimicked PS construct surfaces. Knowing that larger droplet size would exhibit a lower roll off angle, the droplets (~4 -10 μL) on natural lily leaf surface gave roll-off angle (α) ranges, $\alpha_{\parallel} \sim 23^{\circ} - 8^{\circ}$, $\alpha_{\perp} \sim 41^{\circ} - 16^{\circ}$ along parallel and perpendicular directions, respectively. Apparently, adhesion in the parallel direction is relatively weaker than perpendicular direction. The lotus leaf shows roll-off angle range, ~23°-7° when droplet volume was changed between ($\sim 2 - 10\,\mu L$). The bio-mimicked PS surface offers roll-off angles, $\alpha_{\parallel} \sim 49^{\circ} - 21^{\circ}$ and $\alpha_{\perp} \sim 55^{\circ} - 40^{\circ}$ for the droplet size range, ~6-10 μL (Fig. 4.6(d)). The dynamical WCA profile for the droplet size (~6 μL) with varied tilting angles can be found in Figs. 4.7(a) and 4.7(b) meant for natural lily surface, lotus leaf, and bio-mimicked PS construct; respectively. Considering similar droplet sizes of ~6 μL, the respective CAHs for these systems were measured to be ~17.2° (and ~40.6°) and ~25° (and ~50.3°) in parallel (and perpendicular) directions. In a range of droplet volume size ~4-10 μL, the respective CAHs for the leaf specimen ranged, ~16°-41° and ~15°-50° along parallel and perpendicular directions. In contrast, the CAH offered by the bio-mimicked PS construct was seen

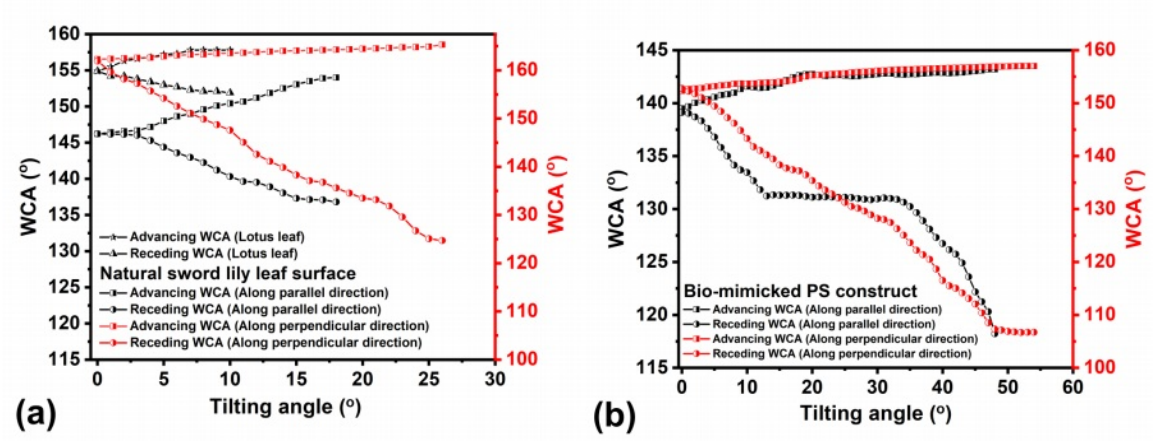

Figure 4.7: (a, b) The dynamic WCA (drop size ∼6 μL) vs. tilting angle plots along parallel and perpendicular directions and for natural adaxial lily leaf and bio-mimicked PS construct surfaces, respectively. Also, for lotus leaf surface, the dynamic WCA with tilting angle is shown in (a) as reference.

to be, ∼20°-39° and ∼50°-56° along the aforesaid directions. The dynamic water droplet state for the droplet size (∼6 μL) with varied tilting angles can be found in Figs. 4.8 and 4.9 for natural lily surface and bio-mimicked PS construct; respectively.

When the droplets roll, quite effortlessly along a guided direction due to specific arrangement of micro-nano texture, it is termed as directional rolling (i.e., directional self-cleaning, see Appendix II, (Fig. A.10)). The rolling droplet with tilting angle on natural lily leaf and bio-mimicked PS construct shows directional self-cleaning along parallel direction taking advantage of highly organised striated waxy construct. It should be noted here that, the WCAs along perpendicular direction in both the cases of natural lily leaf surface and bio-mimicked PS construct are greater than their respective values along parallel direction. Nevertheless, the droplet roll-off along parallel direction is favourable due to the fact that along the parallel direction, the TCL would move forward without any barrier until equilibrium is reached [17]. In perpendicular direction, the edges of micro-striation would act as barrier to moving TCL. To be mentioned, the bio-mimicked PS construct did not show roll-off for the ∼4 μL droplet size and thus it is apparent that the natural leaf texture certainly gives a better droplet roll-off condition undoubtedly due to exceptional structural precision and chemical perfection of nature.

4.4.3 Theoretical analysis on wettability of underneath microtexture

We invoke Cassie- Cassie wetting state to be exhibited by the sword lily leaf surface which offers superhydrophobicity and self-cleaning feature. The difference between lotus and lily leaf surfaces lies in their unique microstructural characteristics. The lily leaf exhibits apparent anisotropic superhydrophobicity and unidirectional self-

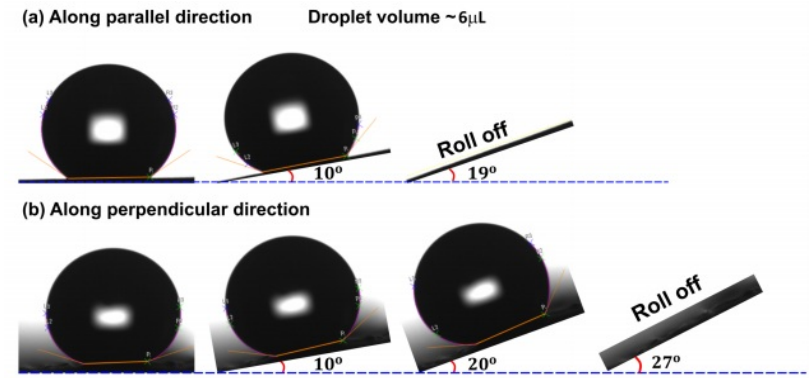

Figure 4.8: The dynamic water droplet state on natural sword lily leaf surface with slanting specimen stage. (a) Along parallel direction, roll-off angle 19°. (b) Along perpendicular direction, roll-off angle 27°.

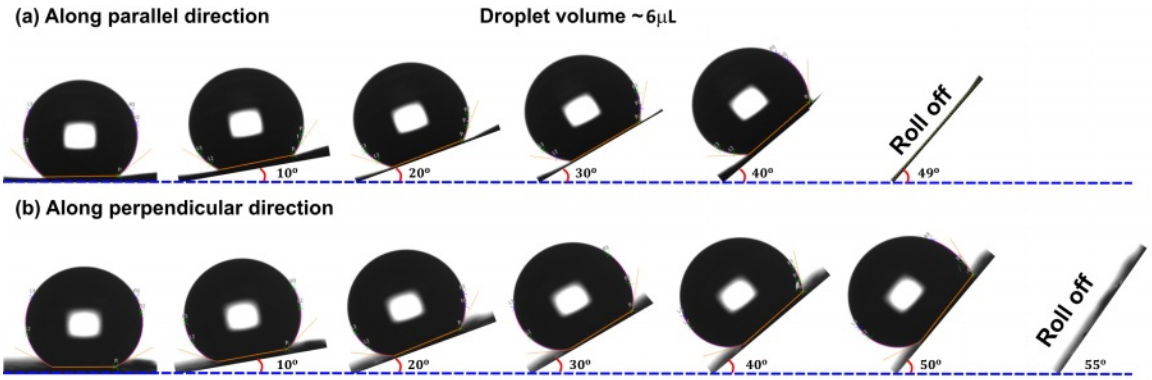

Figure 4.9: The dynamic water droplet state on biomimicked PS construct with tilting specimen stage. (a) Along parallel direction, roll-off angle 49°. (b) Along perpendicular direction, roll-off angle 55°.

cleaning action arisen due to the striated three-level nano-micro surface structure. Whereas, the lotus leaf surface appears with a uniform distribution of micro-nano structures, resulting in an isotropic surface wetting state. The optical image of the droplet wetting state on the natural lily leaf surface can be found in Fig. 4.10(a) and the schematic of the wetting state at sites of micro-protrusions shown in Fig. 4.10(b). It essentially characterizes a situation with micro-protrusions covered with waxy nano flakes and thus the water rests over both the entities. To be mentioned, the trapped air underneath water creates Laplace pressure at the water-air interface, as the water droplet size is much larger, i.e., droplet height $\gg$ capillary length $\left(=\sqrt{\frac{\gamma_{LA}}{\rho g}}\right)$, the sagging effect may take place at water- micro scale texture interface [27, 197]. To avoid gravitational effect on droplet shape, the water droplet size is normally chosen in range of $\sim 4-10\,\mu L$ for self-cleaning measurements. The apparent WCA due to surface texture would give dual suspended wetting regime, i.e., Cassie- Cassie suspended state on the leaf surface. Mathematically, when the droplet is suspended

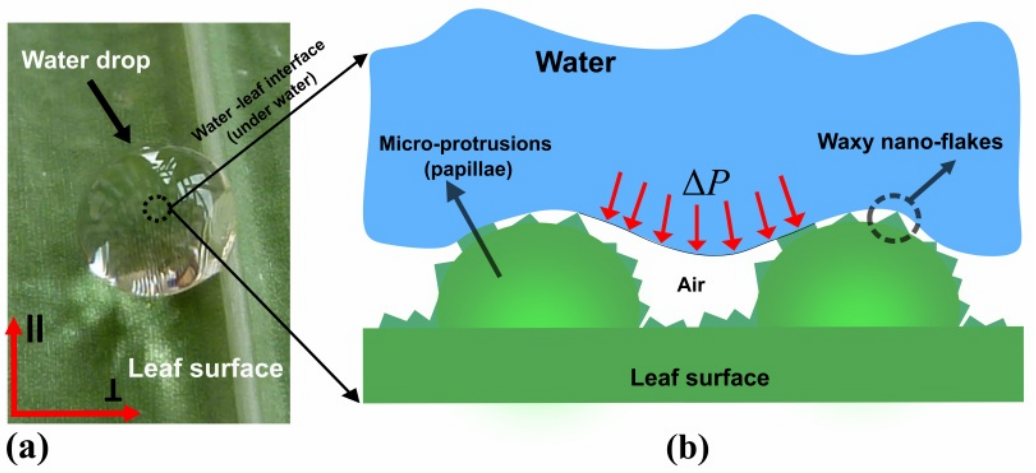

Figure 4.10: (a) Top view of the wetting states of water droplet on adaxial lily leaf surface (optical image). The dotted circle (black) indicates a region of water -leaf interface under water. (b) Schematic of a water-lily leaf surface interface under water offering the Cassie's state. Note the entrapped air being influenced by the uneven nano flakes and consequently, suspended state.

on both micro and nano textures having isotropic wetting state [27], it is given by;

$$\cos\theta_{CC} = f_{\mathrm{M}}\, f_{\mathrm{N}}\,(\cos\theta_{Y} + 1) - 1. \tag{4.1}$$

Where θ_{CC} is the apparent WCA of the Cassie-Cassie state, f_{M} and f_{N} are the fractions of the water droplet contact area with micro and nano scale textures, respectively (see Appendix II, (Fig. A.11)). The θ_{Y} is the Young's WCA on a flat, smooth surface (Ref: Eq. (2.3)). In the present scenario, the Cassie-Cassie model has not validated anisotropic wetting completely because Eq. (4.1) is based on global Gibbs free energy minimization, assuming symmetric motion (spreading) of the water droplet TCL along the solid surface. Given that the surface structure emerges in the form of striation or alignment along a specific direction, the WCA may not remain uniform along the TCL [193, 198].

To explore self-cleaning, the dynamic behavior of the water droplet with base tilting was examined for different droplet volumes ($\sim 4 - 10\,\mu L$). In this regard, Furmidge's equation can be employed, which provides a relationship between the slowing down of the rolling droplet and the slanting angle, without accounting for droplet depinning [125]. The depinning condition of a static water droplet with tilting angle was explained by Brown *et al.* [126]. The tangential force due to gravity along the tilting surface, i.e., the pinning force on the droplet, can be given by [126]:

$$F_p = mg\sin\alpha, \tag{4.2}$$

where mg is the weight of the liquid droplet, and α is the surface tilting angle. At equilibrium, along the inclined surface, this force is balanced by the surface tension exerted along the TCL [127], where the interface between the liquid and air intersects

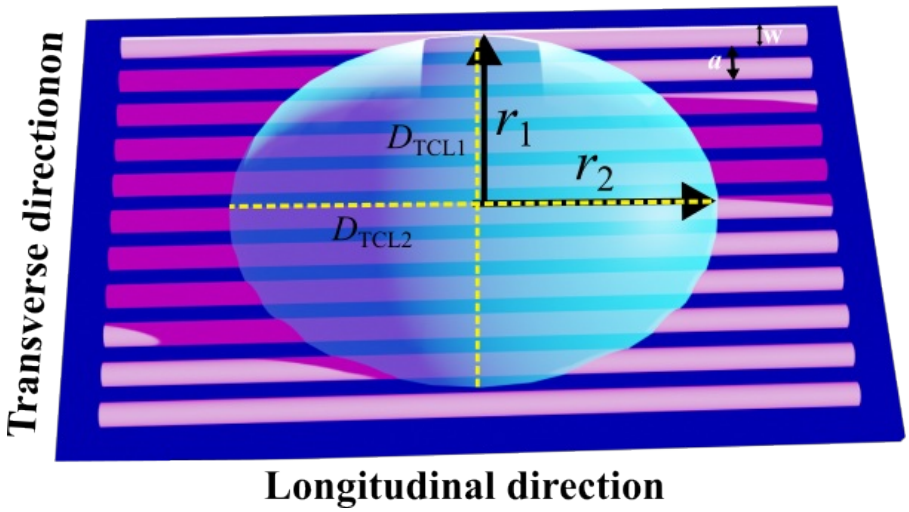

Figure 4.11: Schematic of the anisotropic wetting state on a striated solid surface. Here, r_1 and r_2 represent the minor and major radii of the droplet, respectively, measured perpendicular to the direction of motion. The width of each striation and the separation between successive striations are denoted by a and p, respectively.

with the solid surface. Therefore, the pinning force can be given as:

$$F_p = D_{\mathrm{TCL}}\gamma_{\mathrm{LA}}\left(\cos\theta_r - \cos\theta_a\right). \tag{4.3}$$

The angles θ_r and θ_a characterize the receding and advancing WCAs with tilting angle, α. By combining Eqs. (4.2) and (4.3), one obtains a requisite criterion for the droplet roll-off with tilting angle [128]. It should be noted here that D_{TCL} is the contact line length normal to the direction of droplet motion along the TCL [128, 199]. Consequently:

$$\sin\alpha = \frac{2D_{\mathrm{TCL}}\gamma_{\mathrm{LA}}\left(\cos\theta_r - \cos\theta_a\right)}{\pi mg}. \tag{4.4}$$

Here, the pre-factor $2/\pi$ arises from the droplet shape [125]. Now when the angle of inclination is increased, it might eventually reach a critical tilting angle at which the droplet's weight can no longer be sustained by the tangential surface tension force. Then, the static equilibrium is disrupted, and it allows the droplet to start rolling down the inclined surface. The pinning force can be estimated by Eqs. (4.2) or (4.3), however Eq. (4.4) is generally considered for the isotropic wetting state.

For anisotropic wetting, replace D_{TCL} with the effective contact line length diameter normal to the direction of droplet motion along either the longitudinal or transverse direction (see Fig. 4.11).
On a smooth surface:

- For droplet motion along the longitudinal direction, diameter $D_{\mathrm{TCL}} = 2r_1$,
- For the transverse direction, diameter $D_{\mathrm{TCL}} = 2r_2$.

On a striated (textured) surface, the effective contact line length diameter D_{TCL} is modified due to the presence of grooves. It is given by [200]:

$$D_{\mathrm{TCL1}} = 2r_1 - \frac{2r_1}{a}(a - w), \tag{4.5}$$

or equivalently,

$$D_{\mathrm{TCL1}} = \frac{2r_1 w}{a}. \tag{4.6}$$

Here, a is the pitch distance of the grooves and w is the groove width. The ratio w/a denotes the solid–liquid fractional contact area. Similarly, for the transverse direction:

$$D_{\mathrm{TCL2}} = \frac{2r_2 w}{a}. \tag{4.7}$$

Substituting these expressions into Eq. (4.4), the modified equations become:
For longitudinal direction:

$$\sin\alpha = \frac{4r_1 w\gamma_{\mathrm{LA}}(\cos\theta_r - \cos\theta_a)}{a\pi\rho V g}. \tag{4.8}$$

For transverse direction:

$$\sin\alpha = \frac{4r_2 w\gamma_{\mathrm{LA}}(\cos\theta_r - \cos\theta_a)}{a\pi\rho V g}. \tag{4.9}$$

Thus, Eqs. (4.8) and (4.9) represent an extension of Eq. (4.4), incorporating the effect of the solid-liquid fractional area for single-level microgroove structured surfaces.

Using Eq. (4.2) and an observed roll-off angle, a maximum pining force can be determined for a specific droplet volume. In Fig. 4.6(d), one can observe variation in roll-off angles exhibited by the lotus leaf surface when droplet volume varied in the range, ∼2-10 μL. However, for natural lily leaf surface, the ∼2 μL droplet did not roll -off up to a slanting angle of ∼90°. Similarly, bio-mimicked PS construct displayed a roll -off corresponding to a droplet size of ∼6 μL and above. Accordingly, using Eq. (4.2), the critical pinning forces for natural lily leaf and bio-mimicked PS construct were estimated to be, ∼40 μN and ∼58 μN; respectively. Understanding the magnitude of pinning forces helps in designing and evaluating surfaces for applications requiring specific wetting and self-cleaning properties [128]. As the droplet size increases (i.e., with increasing the droplet weight), the roll-off angle would decline sharply or steadily depending on whether it is more, or less for the minimum droplet size. In fact, a critical tilting (roll-off) angle is needed for a specific droplet size where the tangential pining force must exceed the opposing force on the droplet to set in motion. Along perpendicular direction, striated microstructure heights act as a barrier for the droplet motion due to sufficiently large pinning effect. However,

the parameter which actually resists the motion of TCL on the inclined surface is still debatable [128, 201–204]. Moreover, it was observed that the bio-mimicked PS construct did not support roll-off with ∼4 μL size droplet in both parallel and perpendicular directions, possibly due to predominately stronger pinning force against gravitational force. Also, for droplets of similar sizes, the replicated PS surface experiences a comparatively higher roll-off angle as compared with the natural leaf surface. The observed difference could indeed be influenced by how the TCL transition occurs from a static to a dynamic state, which depends on the local sub-surface constructs and chemical compositions. These factors play a crucial role in determining the wetting behaviour and the effectiveness of self-cleaning mechanisms on both the lily leaf surface and the bio-mimicked PS construct. As mentioned earlier, the bio-mimicked PS construct had a limitation of replicating several nano-scale geometries of the natural lily leaf surface. Additionally, the naturally occurring paraffin waxy surface exhibits a WCA of ∼110°, while the smooth surface of PS stands at a WCA of ∼95° due to its distinct chemical constituents at large [26, 150]. In other words, the natural paraffin wax surface is relatively more hydrophobic in comparison with the smooth PS surface and therefore, adequate hindrance to the movement of TCL can berealized in the latter case.

4.5 Conclusion

- In this work, the anisotropic superhydrophobicity of a three-level surface texture of the sword lily leaf surface has been studied.
- Inspired by three -level surface texture of sword lily leaf, a biomimicked PS replica was cast using a soft lithographic technique.
- The static water contact angles (WCAs) in the parallel ($\theta_{\parallel}$) and perpendicular ($\theta_{\perp}$) directions with altered droplet size (∼4-10 μl) were found as follows:
  (i) Sword lily leaf surface: $\theta_{\parallel} \sim 143° - 147°$, $\theta_{\perp} \sim 156° - 169°$.
  (ii) Bio-mimicked PS construct: $\theta_{\parallel} \sim 130° - 139°$, $\theta_{\perp} \sim 142° - 145°$.
- The dynamic aspects, such as roll-off angles along the parallel ($\alpha_{\parallel}$) and perpendicular ($\alpha_{\perp}$) directions with altered droplet size, were also measured:
  (i) Sword lily leaf surface: $\alpha_{\parallel} \sim 23° - 8°$, $\alpha_{\perp} \sim 41° - 16°$.
  (ii) Bio-mimicked PS construct: $\alpha_{\parallel} \sim 49° - 21°$, $\alpha_{\perp} \sim 55° - 40°$.
- Both surfaces, natural sword lily leaf and PS replica exhibit anisotropic superhydrophobicity adhering to the Cassie model, with exclusive pinning feature in the perpendicular direction.